Fiducial marker detection via deep learning approach for electron tomography

Yu Hao
High Performance Computer Research Center, Institute of Computing Technology
Chinese Academy of Sciences
Beijing, China
haoyu@ict.ac.cn

Fa Zhang*
High Performance Computer Research Center, Institute of Computing Technology
Chinese Academy of Sciences
Beijing, China
zhangfa @ict.ac.cn

Renmin Han
Institute of Computing Technology Computational Bioscience Research Center (CBRC),Computer, Electrical and Mathematical Sciences and Engineering (CEMSE) Division
King Abdullah University of Science and Technology (KAUST)
Thuwal, Saudi Arabia
hanrenmin@gmail.com

Shiwei Sun
Institute of Biophysics
Chinese Academy of Sciences
Beijing, China
dwsun@ict.ac.cn

Xiaohua Wan
High Performance Computer Research Center, Institute of Computing Technology
Chinese Academy of Sciences
Beijing, China
wanxiaohua@ict.ac.cn

***Abstract*—Marker-based alignment widely used for tilt series alignment in electron tomography (ET) is crucial to high-resolution tomographic reconstruction. However, accurate alignment with markers remains a challenge because it is difficult to detect markers accurately and obtain the precise positions of fiducial markers in the tilt series. Conventional marker detection algorithms highly depending on marker template and threshold for classification lack the adaptation for different types of samples. The classification accuracy is severely affected by high contrast structures other than markers and high-density areas. In this paper, we present an automatic fiducial marker detection algorithm that applies a fine-tuned classification model to fit with the particular dataset. The classification via a convolutional neural network (CNN) for marker detection is solved as a binary classification problem distinguishing between the positive samples and negative samples. Also, we established the training data for the model to learn the patterns of the fiducial marker and background noise. The experimental results indicate that our deep learning based marker detection algorithm can identify sufficient fiducial markers with high accuracy in a fully automatic manner and shows superiority compared with previous work.**

Keywords—electron tomography, fiducial marker detection, deep learning, convolutional neural networks

I. INTRODUCTION

Electron tomography (ET) in structural biology is a powerful technique for visualization of macromolecular complexes or cellular structures on a nanoscale. This technique is to reconstruct a three-dimensional volume of an object from its two-dimensional projections in various directions collected on a transmission electron microscope (TEM). Accurate tilt series alignment is essential to high-quality tomographic reconstruction, because the projections suffer inevitable translations, rotations, and magnifications due to the specimen movement, mechanical instabilities and optical imprecisions of the imaging system [1]. The developments of the sub-tomogram averaging (STA) and automatic data collection increase the need for complete automation of alignment for batch tomographic reconstruction.

The alignment of tilt series can be classified into two types: (1) marker-based alignment [2-7] and (2) marker-free alignment [8],[9],[10]. The alignment based on markers, also known as gold beads, is a commonly used alignment method with the highest accuracy which has been applied in ET for decades. The gold beads featuring high-density and circle-shape in 2d projections, benefit the tracking procedure, particularly in low-contrast Cryo-ET samples. Marker detection is the foundation of marker-based alignment to obtain the accurate positions of fiducial markers in the projection images.

Intensive studies have been carried out so far by many investigators focusing on marker detection algorithms [2-6]. In general, these algorithms rely on two inputs, a synthetic or averaged template of golden beads and also a threshold to distinguish the similarity of template and image patches by cross-correlation. The correlation image meeting the threshold indicated that which area is possible to be a marker. S. Brandt et al. [2] evaluated each bead by the shape information of circularity with an artificial template. Although this method was quick and straightforward to perform, the rough template lacked the structural features in current micrograph, and the diameter was measured manually. RAPTOR [6] is a program to implement marker detection by a gradually refined template with a micrograph. The averaged template improved the description of markers, while the bias toward unfair manual sampling was hard to avoid. It was pointed out that beads distributed over dark regions were likely to be left out [3]. A study [3] separated the correlation peak into groups by a background density to judge between beads and non-beads to improve the detection. However, it still had a strong dependence on the radius of markers. The tilt series had to be pre-aligned to get the precise evaluation of the bead' tracking. In light of the above studies, it is hard to determine both the template and threshold since they alter for a diversity of samples under different imaging condition. Cao et al. [7] proposed a marker detector based on gradient analysis. However, the image denoising weakened the performance of the detector. Their assumption was inconsistent with the actual pixel distribution of a marker at high magnification. Moreover, a study demonstrates that none of the marker detection algorithms have the most outstanding performance in all kinds of datasets with various properties [11]. The detection in more complex situations remains an ongoing challenge. For instance, the interference comes from high-density areas, structures other than beads with high contrast to the background, and the inevitable low signal-to-noise ratio.

978-1-5386-5488-0/18/$31.00 ©2018 IEEE

In recent years, the deep learning based approaches have made exciting breakthroughs in a wide range of fields where the conventional computer vision has strived for years. Some successful attempts using CNN models in Cellular electron cryo-tomography (CECT) include a 2D CNN for segmentation of subcellular structures [12], a 3D CNN for segmentation of macromolecules of interest [13], 3D CNNs for classification of macromolecular structure [14]. Thus, our work aims to solve the marker detection as a binary classification problem with a more powerful deep learning based classifier.

Our method shows the following contributions. For one, the training data for our CNN to learn the patterns of fiducial marker and background noise were established by our own. For another, to offer an exhaustive marker detection for a specific dataset, we design a fiducial marker detection algorithm that applies the fine-tuned classification model to increase the scalability without human intervene. The experimental results prove the effectiveness of our method and show superiority compared with previous work.

II. METHODS

Data preparation

Micrographs need to be preprocessed to correct the extreme values deviating from the mean by more than three times standard deviation. Here, both real and synthetic micrographs are used to train our model. Nine sets of tilt series construct a training set with 45613 samples, and another nine sets of tilt series produce a validation set with 7057 samples. The number of positive samples is roughly equal to that of negative samples. As fiducial markers vary in size with different magnifications, the extracted samples are adjusted to fixed 64 pixels x 64 pixels considering the typical dimension of markers, the memory capacity of GPU and the training time. The positive sample is the regions of the single integrate marker with few surrounding pixels, determined by the cross-correlation between patches of a micrograph and an artificial marker template. The negative sample is randomly selected region without markers. All the samples are labeled with ground-truth value. All the samples are shuffled to ensure the randomness and subtract a mean value of training data to save training time. Also, samples are augmented in the manner of random cropping and horizontal mirroring with a probability of 0.5.

The architecture of our convolutional neural network

Referring to the typical architecture of CNNs for ImageNet classification [15], we present a classifier based on a CNN to identify markers among the candidates might be markers. The network comprises five convolutional layers and three fully connected layers that have learnable weights and biases as described in Fig. 1. Except for the final fully connected layers, the output of each layer is activated by rectified linear unit (ReLU) to ensure the nonlinearity of our network. As for convolutional layer, each one a 2D kernel for filtering and a bias for output. The first convolutional layer contains 96 kernels of size 5×5 without padding the edges. The second unpadded convolutional layer has 256 kernels of size 5×5. After each output of the first two convolutional layers, a max pooling layer of 3×3 pixel square with a stride of 2 pixels as well as a Local Response Normalization (LRN) layer is followed. Each last three

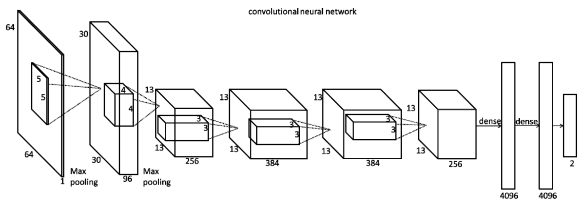

Fig.1. The overall architecture of our CNN.

convolutional layer has 384, 384 and 256 kernels respectively with the size of 13×13 with padding size of 1. The first two fully connected layers apply "dropout" strategy that the neurons are set to zero at the half chance to prevent overfitting. The "dense" operation means an all-to-all connection. Our model feeds the output of the final fully connected layer to a softmax layer with two neurons. Each neuron assigns a probability to the corresponding class. During marker detection, the softmax layer is removed as it weakens extracted features from the final fully connected layer.

Fiducial marker detection based on CNN

Our proposed method employs a CNN to detect the fiducial markers in micrographs, as it is depicted in Fig. 2. The workflow is summarized in the following phases: (1) fine-tuning, (2) candidate marker generation, (3) marker classification, and (4) marker location refinement. Candidate markers generation and refinement follow a similar idea from previous work[5].

Fine-tuning: The pre-trained model needs to get fine-tuned to improve performance on a new given dataset. First, generate the additional training samples for fine-tuning. Both positive samples and negative samples are extracted from five near zero tilts in the current tilt series using template matching. Second, the pre-trained model gets fine-tuned for three epochs. More epochs are proved to make no difference to the fine-tuning.

Candidate marker generation: The diameter of fiducial markers (denoted by d) is assumed to be equal in the identical projection image. It is estimated from a set of synthetic marker templates with multiple diameters to match fiducial markers in the zero-tilt projection image. The two diameters with the highest similarity are picked to diminish the search space until meeting the terminal condition. Furthermore, each slice generates w·h/d2 candidate regions that are sufficient to cover all fiducial markers instead of the sliding window. The theoretical upper bound of fiducial markers is represented by w·h/d2, due to the limitation of micrograph dimensions (the width is denoted by w, and the height is denoted by h) and marker diameter. The peak correlation for each d×d sub-region corresponds to the

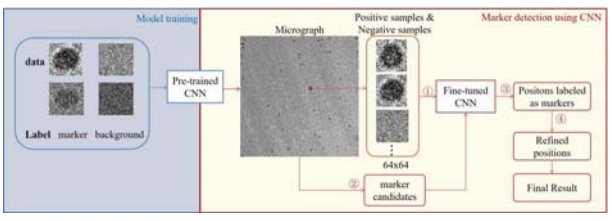

Fig.2. The flowchart of fiducial marker detection solution.

position of a candidate marker.

Classification: The fine-tuned model performs a binary classification for the extracted patch to output a label with a score. The image patches labeled as a marker are reserved, and those labeled as background are discarded.

Refinement: With the assumption that the fiducial markers look alike in the same micrograph, a referenced marker template is derived by averaging the detected markers in a micrograph. The difference between the referenced marker template and detected fiducial markers is continuously reduced by relocating the fiducial markers and generating new referenced marker template until to satisfy the stopping threshold.

Training

Hyper-parameters is vital to train our model more efficiently and make the model not merely perform well on training data but also generalize to new data. The initial learning rate is 0.001 divided by ten every 1000 iterations. Weights are randomly initialized using Gaussian distribution with zero-mean with a standard deviation of 0.005 for first two fully connected layers and 0.01 for remaining layers. The biases in the first, third, and eighth convolutional layer and the last fully connected layer are initialized to the constant 0 and others are initialized to 1. Images are passed through the model with a batch size of 256 in the training phase and a batch size of 64 in the validating phase. A stochastic gradient descent algorithm trains the model with the momentum of 0.95 and weight decay of 0.05 for regularization. In the course of training, both images and labels are imported to the network and processed layer by layer. Loss and gradients deriving from the last layer are used for further training. The model is iteratively optimized by a forward pass and backward pass to update the parameters to minimize the loss function. A set of weights from the current model is saved after one epoch training. The training operation is terminated when validation loss is not improving for at least four consecutive epochs. The current model serves as a basic model to get fine-tuned during detection.

The model was trained and deployed with Caffe, equipped with one Tesla K20c GPU card. It costs about 1.3 minutes to classify more than 1700 markers from a micrograph of size 3710×3838. The training time for ten epochs is about half an hour.

III. Results

Test datasets

We applied the proposed marker detection method to two datasets and compared the results with markerauto [18]. The first dataset, is a tilt series of the 5-HT3 receptor shown in Fig. 3(A), which is collected by Titan Krios(FEI) operated at 300 kV accelerating voltage with a K2 Summit electron detector. 46 tilt series range from -60° to +60° with an increment of 3°. The image dimension is 3710× 3838 with a pixel size of 0.167nm. The marker diameter is about 62 pixels. This data has been deposited in Electron Microscopy Public Image Archive with the accession code EMPIAR-10046(tomo_37.mrc)[16]. The second dataset is a tilt series of the motor shown in Fig. 3(B). There are 41 images collected on FEI Tecnai TF20 (FEI) equipped with a FEG source operated at 200 kV accelerating voltage using a Falcon II direct electron detector. The image size is 2048 × 2048 with a pixel size of 0.4061 nm, tilted from –61° to +61° with 3° tilt increments. The last image was excluded from the tilt series due to the abnormal data acquisition. The diameter of fiducial markers is around 26 pixels. The data has been deposited in Electron Microscopy Public Image Archive with the accession code EMPIAR-10111[17].

Experiments

The detected fiducial markers at the tilt angle of +60°, 0°and -60° are shown in Fig. 4. In Fig. 4(A) and (B), most of the well-distributed fiducial markers with clear shape were detected by our method. The rest markers were not selected because of the incomplete appearance or partial overlapping. Some ignored markers in Fig. 4 (D) and (E) are also detected by our method. In Fig. 4(C) and (F), we observed that a mass of fiducial markers was distributed on the top of the micrographs, the number of overlapped fiducial markers in the field increases, and the appearance of some fiducial markers becomes heavily blur as well as low-contrast as the sample tilts to higher angle. Our method overcame these difficulties at a high tilt to picked out the best ones among all fiducial markers. Fig. 5 compares the track length histograms of detected fiducial markers to assess the performance. Because of the tremendous shift and very high noise in this dataset, it is hard to obtain a long track length. The longest track produced by our method covers 18 of the 41 projection images and showed a slightly better result than markerauto.

The detected markers from three micrographs performed by our method are shown in Fig. 6. The high contrast markers at near zero tilt were easy to be detected as shown in Fig. 6 (B). The misleading dark background and interference factors around the markers in Fig. 6 (A) and (C) are solved well by our method. Fig. 7 illustrates the position tracks of the same fiducial markers before alignment (top) and after

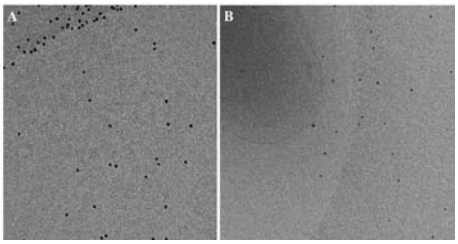

Fig.3. Example micrographs taken at 0° from test datasets. (A) The micrograph of a 5-HT3 receptor. (B) The micrograph of a motor.

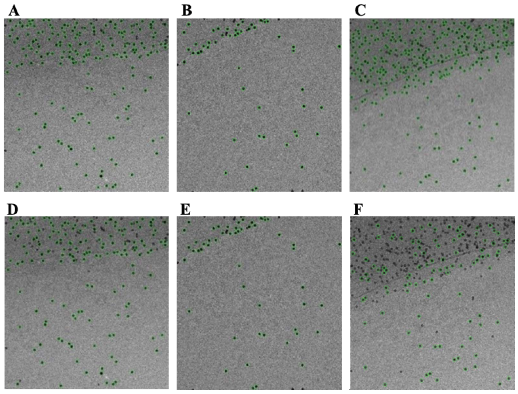

Fig. 4. Illustration of marker detection for the first dataset. All the detected markers circled in green were generated by markerauto (bottom) and our method (top). (A)(D) Detected markers at tilt angle +60°. (B)(E) Detected markers at tilt angle 0°. (C)(F) Detected markers at tilt angle -60°.

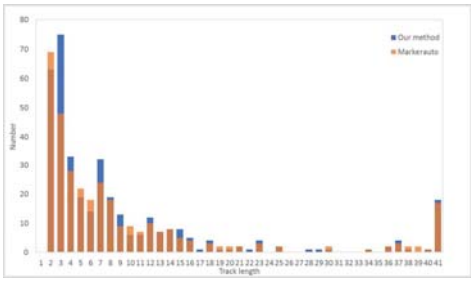

Fig.5. Histograms of the track lengths of assembled markers for the first dataset where the detection part using our method(blue) and markerauto(orange).

alignment(bottom). The markers were first obtained with our detection algorithm, then the markers were matched up between adjacent projections to form longer position tracks. Compare the tracks in Fig. 7(A) and (B), plenty of disordered tracks turned into horizontal lines due to the valid alignment.

IV. Discussion and Conclusion

We have proposed an automatic marker detection based on a CNN classifier for electron tomography, derived from the previous work [5] to achieve a more robust, more accurate and more scalable detection. We carried out several experiments to demonstrate the effectiveness of our detection method. However, the performance of the classifier may get worse when the diameter is merely a few pixels with not enough structural information. In the future work, we can attach more importance to the predicted score for each marker to optimize the projection parameter estimation. It is a worthwhile attempt to eliminate the reconstruction artifacts caused by markers in a deep learning way.

Acknowledgment

This research is supported by the National Key Research and Development Program of China (No. 2017YFA0504702 and 2017YFE0103900), the NSFC projects Grant (No. U1611263, U1611261, 61472397, 61502455 and 61672493) and Special Program for Applied Research on Super Computation of the NSFC-Guangdong Joint Fund (the second phase).

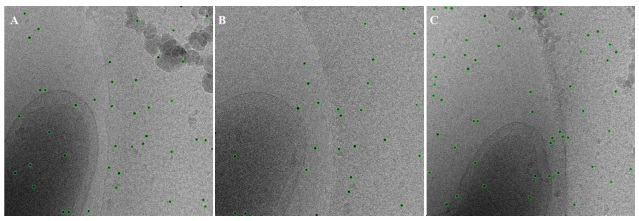

Fig.6. Illustration of detected markers circled in green for the second dataset. (A) Detected fiducial markers from the 3rd micrograph. (B) Detected markers from the 21st micrograph. (C) Detected markers from the 37th micrograph.

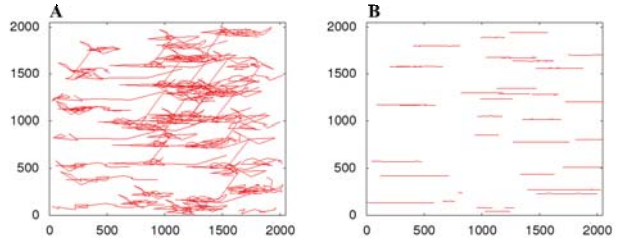

Fig.7. Illustration of alignment by our method for the second dataset (2048×2048). (A) Overlay of unaligned marker positions tracked through all tilt angles in image space (x-y coordinates in pixel). (B) Overlay of aligned marker positions tracked through all tilt angles in image space (x-y coordinates in pixel).

References

[1] J. Frank, Electron Tomography: Methods for Three-Dimensional Visualization of Structures in the Cell, Springer Science & Business Media, 2006.

[2] S. Brandt, J. Heikkonen, and P. Engelhardt, "Multiphase method for automatic alignment of transmission electron microscope images using markers" , Journal of Structural Biology, vol. 133, no. 1, pp. 10-22, January 2001.

[3] D.N. Mastronarde, and S. R. Held, "Automated tilt series alignment and tomographic reconstruction in IMOD" , Journal of Structural Biology, vol. 197, no. 2, pp. 102–113, February 2017.

[4] D. Ress, M. L. Harlow, M. Schwarz, R. M. Marshall, and U. J. Mcmahan, "Automatic acquisition of fiducial markers and alignment of images in tilt series for electron tomography" , Journal of Electron Microscopy, vol. 48, no. 3, pp. 277-287, January 1999.

[5] R. Han, L. wang, Z. Liu, F. Sun, F. Zhang, "A novel fully automatic scheme for fiducial marker-based alignment in electron tomography" , Journal of Structural Biology, vol. 192, no. 3, pp. 403–417, December 2015.

[6] F. Amat, F. Moussavi, L. R.Comolli, G. Elidan, K. H. Downing, and M. Horowitz, "Markov random field based automatic image alignment for electron tomography", Journal of Structural Biology, vol. 161, no. 3, pp. 260-275, March 2008.

[7] M. Cao, A. Takaoka, H. B. Zhang, and R. Nishi, "An automatic method of detecting and tracking fiducial markers for alignment in electron tomography", Journal of Electron Microscopy, vol. 60, no. 1, pp. 39-46, February 2011.

[8] S. Brandt, J. Heikkonen, and P. Engelhardt, "Automatic alignment of transmission electron microscope tilt series without fiducial markers", Journal of Structural Biology, vol. 136, no.3, pp. 201–213, December 2001.

[9] L. Yu, P. A. Penczek, B. F. Mcewen, and J. Frank, "A marker-free alignment method for electron tomography", Ultramicroscopy, vol. 58, no. 3-4, pp. 393–402, June 1995.

[10] R. Han, F. Zhang, X. Wan, J. J. Fernández, F. Sun, and Z. Liu, "A marker-free automatic alignment method based on scale-invariant features", Journal of Structural Biology, vol. 186, no. 1, pp. 167–180, February 2014.

[11] T. Patrick, B. Sviatoslav, D. Tim, and S. Philipp, "A comparative study of three marker detection algorithms in electron tomography", Microscopy & Microanalysis, vol. 22, no. S3, pp. 1044-1045, July 2016.

[12] M. Chen, W. Dai, S. Y. Sun, D. Jonasch, C.Y. He, M. F. Schmid, W. Chiu, and S. J Ludtke, "cc", Nature Methods, vol. 14, no. 10, pp. 983-985, October 2017.

[13] C. Liu, X. Zeng, R. Lin, X. Liang, Z. Freyberg, E. Xing, and M. Xu, "Deep learning based supervised semantic segmentation of electron cryo-subtomograms", arXiv preprint arXiv : 1802.04087,2018.

[14] C. Che, R. Lin, X. Zeng, K. Elmaaroufi, and J. Galetti, "Improved deep learning-based macromolecules structure classification from electron cryo-tomograms", Machine Vision & Applications, pp. 1-10, 2017.

[15] A. Krizhevsky, I. Sutskever, and G. E. Hinton, "ImageNet classification with deep convolutional neural networks", International Conference on Neural Information Processing Systems, Curran Associates Inc, vol. 60, pp.1097-1105, December 2012.

[16] A. Iudin, P. K. Korir, J. Salavert-Torres, G. J. Kleywegt, and A. Patwardhan, "Empiar: a public archive for raw electron microscopy image data", Nature Methods, vol. 13,no. 5, pp. 387, March 2016.

[17] M. Beeby, D. A. Ribardo, C. A. Brennan, E. G. Ruby, G. J. Jensen, and D. R. Hendrixson, "Diverse high-torque bacterial flagellar motors assemble wider stator rings using a conserved protein scaffold", Proceedings of the National Academy of Sciences of the United States of America, vol. 113, no. 13, pp. E1917-26, March 2016.

[18] R. Han, , F. Zhang, X. Gao, "A fast fiducial marker tracking model for fully automatic alignment in electron tomography", Bioinformatics, vol. 34, no. 5, pp. 853-863, March 2018.